Biosensors and Bioelectronics 36 (2012) 41–47

Contents lists available at SciVerse ScienceDirect

Biosensors and Bioelectronics

journal homepage: www.elsevier.com/locate/bios

Fabrication of hydrogen peroxide biosensor based on Ni doped SnO_2 nanoparticles

N. Lavanya, S. Radhakrishnan, C. Sekar *

Department of Bioelectronics and Biosensors, Alagappa University, Karaikudi 630003, Tamilnadu, India

ARTICLE INFO

Article history:
Received 23 December 2011
Received in revised form
6 March 2012
Accepted 23 March 2012
Available online 10 April 2012

Keywords:
Tin oxide
Ni doping
Microwave irradiation
Hydrogen peroxide
Biosensors

ABSTRACT

Ni doped SnO_2 nanoparticles (0–5 wt%) have been prepared by a simple microwave irradiation (2.45 GHz) method. Powder X-ray diffraction (XRD) and transmission electron microscopy (TEM) studies confirmed the formation of rutile structure with space group (P_{42}/mnm) and nanocrystalline nature of the products with spherical morphology. Direct electrochemistry of horseradish peroxidase (HRP)/nano-SnO_2 composite has been studied. The immobilized enzyme retained its bioactivity, exhibited a surface confined, reversible one-proton and one-electron transfer reaction, and had good stability, activity and a fast heterogeneous electron transfer rate. A significant enzyme loading (3.374×10^{-10} mol cm^{-2}) has been obtained on nano-Ni doped SnO_2 as compared to the bare glassy carbon (GC) and nano-SnO_2 modified surfaces. This HRP/nano-Ni–SnO_2 film has been used for sensitive detection of H_2O_2 by differential pulse voltammetry (DPV), which exhibited a wider linearity range from 1.0×10^{-7} to 3.0×10^{-4} M (R=0.9897) with a detection limit of 43 nM. The apparent Michaelis–Menten constant (K_M^{app}) of HRP on the nano-Ni–SnO_2 was estimated as 0.221 mM. This excellent performance of the fabricated biosensor is attributed to large surface-to-volume ratio and Ni doping into SnO_2 which facilitate the direct electron transfer between the redox enzyme and the surface of electrode.

1. Introduction

Nanostructured metal oxide semiconductors possesses high surface area, nontoxicity, good biocompatibility, sensitivity, and chemical stability that can easily be modified for immobilization of biomolecules for biosensor applications (Ansari et al., 2010). Among the metal oxide semiconductors, tin oxide (SnO_2), an n-type semiconductor with a wide band gap of 3.6 eV at 300 K, has been investigated for various applications such as gas sensors, solar cells, transparent conductive electrodes, spintronics and biosensor etc. (Chu et al., 2011; Ahn et al., 2004). One of the most important methods to modify the materials is the introduction of dopants into host system. A numerous experimental investigations have been performed on SnO_2 doped with transition metal ions such as Co, Mn, Fe, Ni, and Cr. Among these, Ni is of special interest because of its capability of grain growth inhibition within the SnO_2 matrix (Jain et al., 2006). Pure and doped SnO_2 have been produced using various techniques such as sol gel method (Sambasivam et al., 2011), solid state reaction method (Ahmed. 2010), spray pyrolysis (Korotcenkov and Do Han, 2009), chemical vapor deposition method (Zhang et al., 2010), solvothermal method (Kang et al., 2007), polymer precursor method (Aragon et al., 2010), etc.

In recent years, sensitive and accurate determination of hydrogen peroxide (H_2O_2) is of great importance, because H_2O_2 is not only a byproduct of several selective oxidases but also an essential mediator in food, industry, pharmaceutical laboratories and environmental analyses (Lin et al., 2010). Many techniques have been employed for the determination of H_2O_2, which includes spectrophotometry (Lobnik and Cajlakovic 2001), chemiluminescence (Janasek et al., 1998), and electrochemistry (Kafi et al., 2008). Among these, electrochemistry has been widely applied for accurate determination of H_2O_2. Many proteins have been employed to construct the potential H_2O_2 biosensors, such as HRP, cytochrome C, myglobin and hemoglobin which are capable of reducing H_2O_2 electro catalytically. HRP is the most commonly used enzyme for the construction of H_2O_2 biosensors due to its high purity, sensitivity and low cost (Ferapontova et al., 2002). Cao et al. investigated the direct electrochemistry of heme protein immobilized on Fe_3O_4 nanoparticles for highly reproducible H_2O_2 sensing (Cao and Hu, 2006). Li et al. reported the Sb doped SnO_2 nanowires to possess excellent electron transfer properties for the enzymes than that of pure SnO_2 nanowire (Li et al., 2010a, 2010b). The electro catalytic ability of HRP–TiO_2 nanotube arrays had different sensitivities to H_2O_2 due to their different conductivity (Xiao et al., 2007). Ansari et al. have applied

* Corresponding author. Tel.: +91 94425663637; fax: +91 4565 225202.
E-mail address: Sekar2025@gmail.com (C. Sekar).

0956-5663/$ - see front matter © 2012 Elsevier B.V. All rights reserved.
http://dx.doi.org/10.1016/j.bios.2012.03.035

nanostructured CeO_2 film deposited onto indium-tin-oxide (ITO) glass substrate for immobilization of HRP via physiosorption technique for H_2O_2 reduction (Ansari et al., 2009). Lu et al., have developed porous nanosheet-based ZnO microspheres for the construction of direct electrochemical H_2O_2 biosensor (Lu et al., 2008). Currently, many reports are available for the amperometric detection of H_2O_2 based on enzymatic reaction. However, they have generally used expensive nanomaterials such as MWCNT (Wan et al., 2009), Au (Yin et al., 2009) and Ag (Song et al., 2010a, 2010b) etc. and involve complex multiple step for enzyme immobilization.

In this work, we prepared SnO_2 and Ni doped SnO_2 nanoparticles by a simple and efficient microwave irradiation method. The time required for synthesis was around 10 min only. These nanoparticles modified electrodes provide a well-defined microenvironment for enzyme (HRP) immobilization and enhanced the direct electron transfer between HRP and electrodes. Interestingly, the electron transfer ability of nano-Ni–SnO_2 sample was found to be higher than that of pure SnO_2 as revealed by electrochemical impedance spectoscopy (EIS) and cyclic voltammetry (CV) measurements. Further, the HRP immobilized with nano-Ni–SnO_2 facilitate the good communication between electrode and HRP and it accommodates higher concentration of HRP on the electrode surface compared to that of pure SnO_2 and bare electrode surfaces. These results demonstrate application of the fabricated metal oxide based biosensors for electrochemical detection of H_2O_2. To the best of our knowledge, this is first report on the preparation and applications of Ni doped SnO_2 nanoparticles as H_2O_2 sensor. This work may provide new insight into the preparation of other enzymatic biosensors.

2. Experimental

2.1. Materials

Horseradish peroxidase (HRP) (EC 1.11.1.7, type V1-A, 250–330 units/mg, lyophilized powder from Amoracia rusticana) was obtained from Sigama. $NiCl_2 \cdot 6H_2O$ (Fischer) and $SnCl_2 \cdot 2H_2O$, 30% H_2O_2 aqueous solution were purchased from SDF Co. Ltd. (Mumbai). All other reagents were of analytical grade and used without further purification. The 0.1 M phosphate buffer solution (PBS) with different pH values were prepared by mixing the stock standard solutions of Na_2HPO_4 and NaH_2PO_4 and adjusting the pH with 0.1 M H_3PO_4 or NaOH. The solutions were prepared with double-distilled water.

2.2. Instrumentation

A CHI 6005D electrochemical analyzer (CH Instuments, Austin, USA) connected to a glassy carbon working electrode (0.07 cm^2), saturated calomel electrode (SCE) reference electrode and a platinum wire auxiliary electrode was used. All the solutions were deaerated with inert nitrogen gas during experiments. Cyclic voltammetry (CV) were recorded between a potential window −0.2 and 0.7 V at a scan rate of 50 mV/s in 0.1 M KCl containing 1.0 mM $[Fe(CN)_6]^{3-/4-}$ redox couple. Electrochemical impedance spectroscopy (EIS) measurements were performed in presence of 0.1 M KCl solution containing 1.0 mM $[Fe(CN)_6]^{3-/4-}$ at a bias potential of 0.2 V by applying ac voltage with a 5 mV amplitude in the frequency range from 100 Hz to 1 Hz. Resulting impedance data are presented in Nyquist plots and charge transfer resistance (R_{CT}) values were obtained by simulation of Zsimwin software. The differential pulse voltammetry (DPV) measurements were performed using an Autolab (model PGSTAT302 from Netherlands). The potential was scanned in the range from −0.7 and 0.0 V in PBS (pH 7.0) at scan rate 10 mV/s and the modulation amplitude was 25 mV.

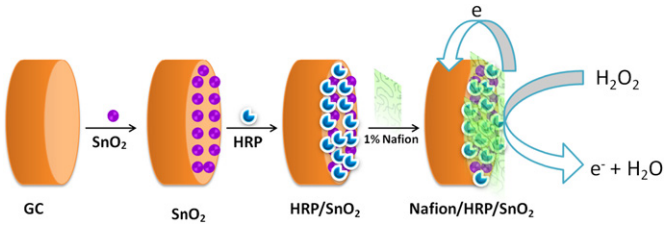

Scheme 1. H_2O_2 detection scheme using HRP/SnO_2 modified glassy carbon electrode.

Powder X-ray diffraction patterns of the samples were recorded using a Bruker AXS D8 advanced diffractometer with CuKα radiation ($\lambda = 1.5406$ Å) in the range 20–80°. Transmission Electron Microscopy (TEM) pictures were recorded on a Technai G20-stwin using an accelerating voltage of 200 kV. Magnetization versus applied magnetic field (*M–H*) measurement at room temperature was undertaken using Vibrating Sample Magnetometer (Model: P252 Quantum Design). The specific surface area of the samples was determined from Brunauer–Emmett–Teller (BET) adsorption measurements using Quantachrome instruments.

2.3. Materials preparation

We have prepared Ni doped SnO_2 (0–5 wt%) powders by using microwave irradiation method for the first time. All the reagents used were of analytical grade without further purification. 0.1 M solution of $SnCl_2 \cdot 2H_2O$ and $NiCl_2 \cdot 6H_2O$ were prepared using de-ionized water as a solvent. Ammonium hydroxide (NH_4OH) solution was added drop wise until the pH of the solution reached 8. After 30 min stirring, a light greenish colloidal solution was obtained which was washed with de-ionized water several times in order to remove chlorine ions. Further the precipitate was washed with ethanol to remove NH_4^+ ions. The washed precipitate was exposed to microwave irradiation with the frequency and power of 2.45 GHz and 600 W respectively. Final black color powder was annealed at 600 °C for 5 h in ambient atmosphere in order to prepare Ni–SnO_2 powders with improved crystallinity.

2.4. Electrode preparation and modification

A glassy carbon (GC) electrode was polished with 1.0, 0.3 and 0.05 μm alumina powder, and then sonicated in ethanol and water each for 5 min. The modified electrodes were prepared by a simple drop casting method. Typically, 10 μL of metal oxide nanoparticles (5 mg/mL) suspension was mixed with 10 μL of HRP (4 mg/mL, 0.1 M PBS, pH 7.0) solution. Then, 10 μL of the mixed dispersion was cast onto the GC electrode, dried at room temperature; the electrode was rinsed in 0.1 M PBS (pH = 7.0) to remove the unbound HRP. Subsequently 5 μL of 1% Nafion solution was dropped over the HRP- nano-SnO_2 modified surfaces to form a tight membrane on the surface (scheme 1). The modified electrodes were rinsed with PBS and stored at 4 °C in refrigerator when not in use. To investigate the electrochemical property of enzyme modified film, cyclic voltammetry (CV) has been performed in PBS (pH 7.0) with the potential range between −0.7 and 0.0 V at a scan rate of 100 mV/s.

3. Results and discussion

3.1. Structural analysis

Powder X-ray diffraction patterns of Ni–SnO_2 (0–5 wt%) samples are shown in Fig. 1(A). All the peaks could be indexed to the

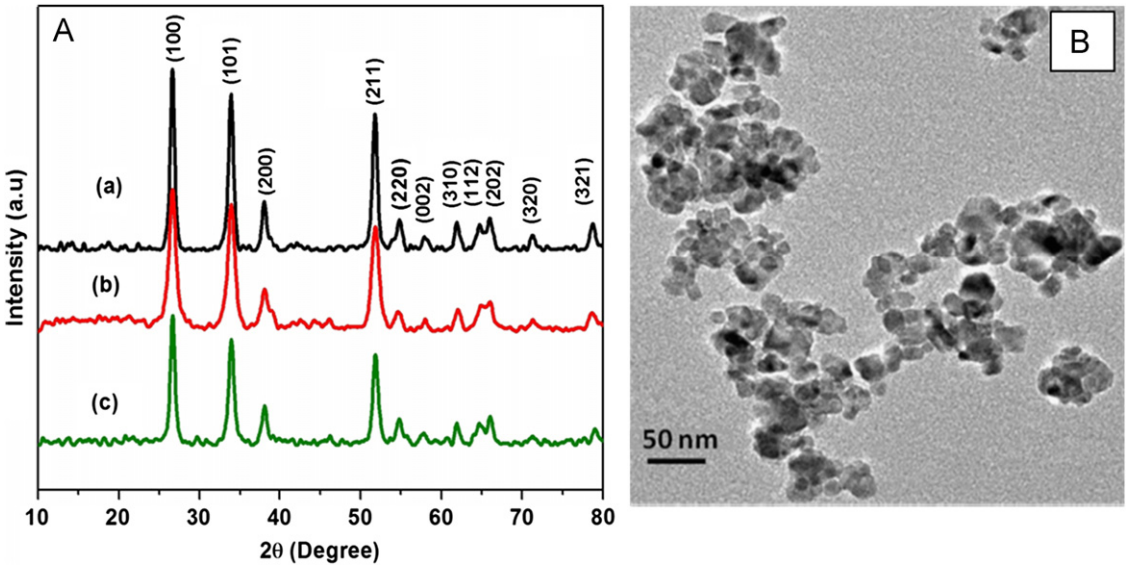

Fig. 1. (A) XRD pattern of (a) pristine SnO_2, (b) 1 wt% and (c) 5 wt% of Ni doped SnO_2 and (B) shows TEM image of pristine SnO_2.

tetragonal system under rutile structure of nano-SnO_2 with space group (P_{42}/mnm). No additional peaks corresponding to possible impurity phases such as NiO, Ni_2O_3, SnO, Ni was observed in the XRD pattern up to the resolution limit of the experiment. Hidalgo Falla et al. have reported the occurrence of traces of NiO in the Ni doped SnO_2 for the excessive dopant concentration of 50 wt% Ni (Hidalgo Falla et al., 2004). In the present study, we have used a maximum of 5 wt% Ni only as dopant. Thus the Ni doped SnO_2 can be expected to be phase pure. The average crystallite sizes were calculated using Debye Scherrer formula

$$D = 0.9\lambda/\beta\cos\Theta$$

where β is the full width at half maximum (FWHM) in radian of the peak with given (hkl) value, $\lambda = 1.5406$ Å of the CuKα radiation and Θ is the diffracting angle. The average crystallite sizes were found to be 19, 14, and 9 nm for pristine SnO_2, 1 wt% and 5 wt% Ni doped SnO_2 respectively. There is no significant change in the lattice parameters and cell volume possibly due to the nearly equal size of dopant Ni ion (0.69 Å) with that of host ion Sn (0.71 Å). However, upon increasing the Ni content, a moderate decrease in the intensity of diffraction peaks, accompanied by a pronounced broadening, has been observed. In the first approximation, this can be attributed to the decrease of particle size, doping of SnO_2 with Ni through the formation of a Ni–Sn solid solution and/or to the induced microstrain. Indeed, when Ni is doped into SnO_2, complicated defect-systems may form, i.e. interstitial Ni and Sn, as well as oxygen vacancy defects could exist, apart from Ni substituting Sn, through substitutional or interstitial doping. The XRD data of Ni-doped samples indicate that SnO_2 is still mainly in the rutile phase, suggesting a substitutional doping of Ni at Sn-site. In this case, based on the *Kroger–Vink* notations, the oxygen-ion vacancies ($V_o^{\bullet\bullet}$) created by substitutional doping of Sn^{4+} with Ni^{2+} are charge compensated by electron holes ($h^{\bullet}$), when the sample is annealed in air. TEM studies indicated that both the pristine and Ni doped SnO_2 formed as spherical nanoparticles and that the particle sizes decreases due to Ni doping. Fig. 1(B) shows the representative TEM picture of pristine SnO_2 nanoparticles.

3.2. Magnetic measurements

In order to understand the role of magnetic Ni ion impurity on the sensing characteristics of SnO_2, we have carried out magnetic measurements using vibrating sample magnetometer (VSM). Room temperature magnetization behavior (M–H curves) of Ni–SnO_2 nanoparticles (0–5 wt%) is shown in Fig. 2. Pristine nano-SnO_2 showed diamagnetic behavior with negative susceptibility. This behavior arises due to the 4+ valance state of tin (Sn^{4+}) which favors $4d^{10}$ electronic configuration in SnO_2 and hence, there is no unpaired d electrons in the structure for any kind of ferromagnetic ordering (Tian et al., 2008). Subsequent Ni doping (1 wt%) did not change the diamagnetic nature of the SnO_2 but with higher Ni content (5 wt%), the diamagnetic order is gradually substituted by a paramagnetic contribution. For 5 wt% Ni, hysteresis loop is observed, which revealed ferromagnetic ordering with a saturation magnetization and coercive field of $M_S \sim 2.0 \times 10^{-3}$ emu/g and $H_C \sim 1.2$ kOe, respectively.

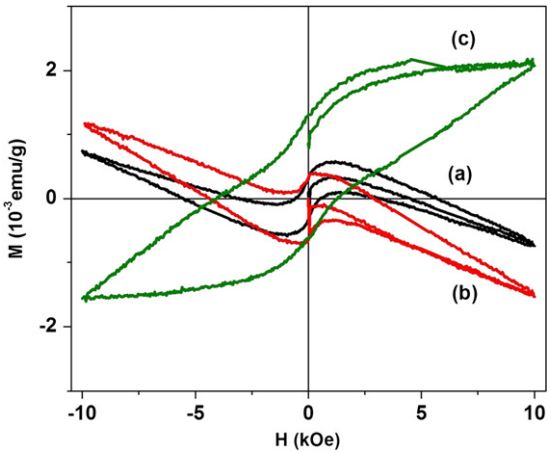

Fig. 2. Magnetization (M) vs. magnetic field (H) curves obtained for pristine (a) pristine SnO_2, (b) 1 wt% and (c) 5 wt% of Ni doped SnO_2.

3.3. Electrochemical activity of SnO_2 nanoparticles modified GC electrode

Electron transfer properties of the GC electrode after surface modification were characterized by EIS. The charge transport processes in nano-SnO_2 modified electrode was studied by monitoring charge transfer resistance (R_{CT}) at the electrode/electrolyte interface. The value of electron transfer resistance

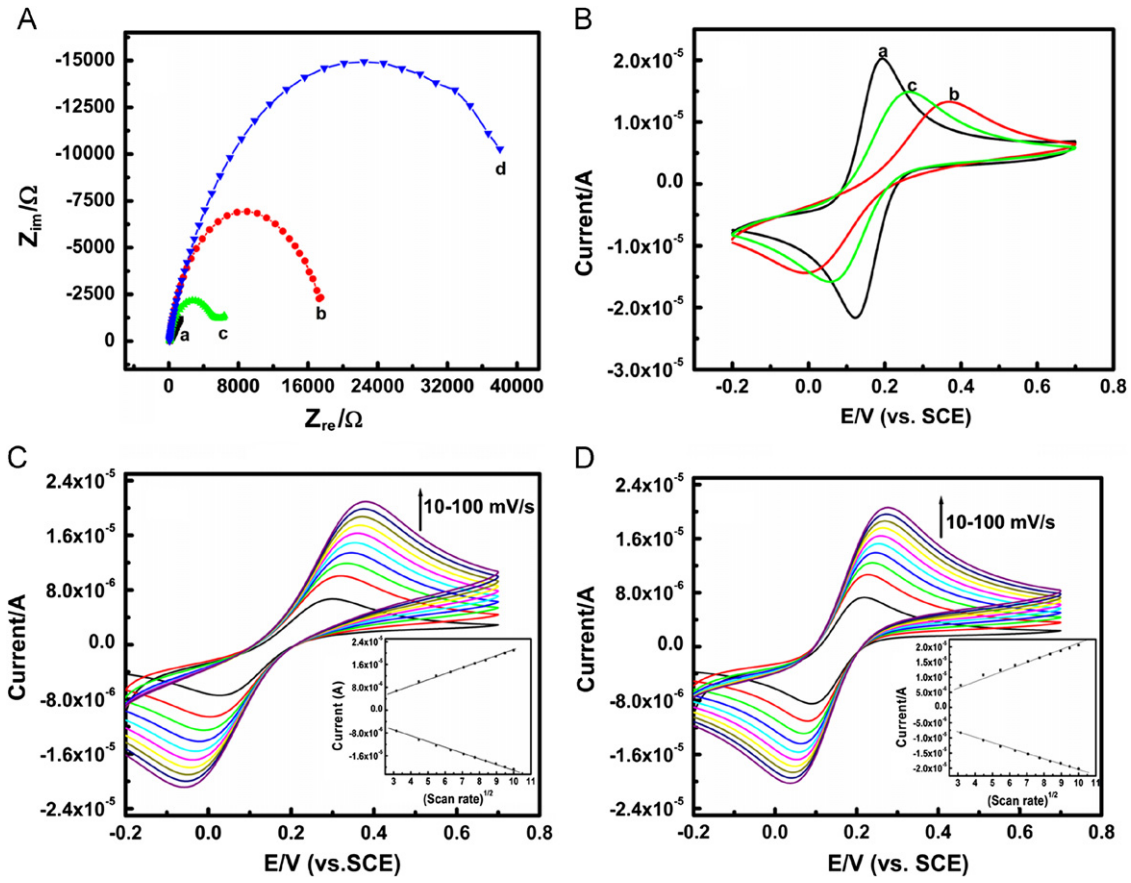

Fig. 3. (A) Electrochemical impedance spectra of (a) bare GC, (b) pristine SnO_2, (c) 1 wt%. Ni doped SnO_2 and (d) 5 wt% Ni doped SnO_2 recorded at the DC potential 200 mV, AC potential ± 5 mV in presence of 0.1 M KCl solution containing 1 mM $[Fe(CN)_6]^{3-/4-}$. (B) Cyclic voltammograms (CVs) of (a) bare GC, (b) pristine SnO_2, and (c) 1 wt% Ni doped SnO_2 modified GC electrodes in 0.1 M KCl containing 1 mM $[Fe(CN)_6]^{3-/4-}$ measured at a scan rate of 50 mV/s; (C) CVs of pristine SnO_2 and (D) CVs 1 wt% Ni doped SnO_2 modified GC electrodes are shown as a function of scan rate (10–100 mV/s). Inset shows plots of peak current vs. square root of scan rate in 0.1 M KCl containing 1 mM $[Fe(CN)_6]^{3-/4-}$.

depends on the dielectric and insulating features at the electrode/electrolyte interface. The Nyquist plot of impedance spectra includes a semicircle portion and linear portion. The semicircle portion at higher frequencies corresponds to the diffusion process. Fig. 3(A) shows the EIS curves of the bare and modified GCEs. The value of charge-transfer resistance (R_{CT}) for bare GC, nano-SnO_2, 1 wt% and 5 wt% Ni doped nano-SnO_2 modified electrodes have been estimated as 161, 16650, 4984 and 35010 $\Omega\,cm^{-2}$, respectively. The R_{CT} value of 1 wt% Ni doped nano-SnO_2 is 7.0 and 3.3 fold lower than that of the 5 wt% Ni doped SnO_2 and pristine samples respectively. Upon increasing the Ni content to 5 wt%, R_{CT} value increases in agreement with the fact that Ni^{2+} substitution at Sn^{4+} site minimizes electron density in the n-type semiconductor SnO_2. We have used 1 wt% Ni doped SnO_2 nanoparticles for further investigations and it is represented as nano-Ni–SnO_2.

Further evidence was obtained from cyclic voltammetry (CV) measurements of the nano-SnO_2 and nano-Ni–SnO_2 modified electrodes [Fig. 3(B)]. The cyclic voltammograms (CVs) were recorded at 50 mV/s for (a) bare GC, (b) nano-SnO_2 and (c) nano-Ni–SnO_2 modified electrodes in 0.1 M KCl containing 1 mM of $[Fe(CN)_6]^{3-/4-}$. At the bare GC electrode, a pair of well defined redox peaks was observed with the peak separation of 70 mV ($\Delta E_p = (E_{pa} - E_{pc})$). But for the nano-$SnO_2$ modified electrode, the CV response was severely suppressed with a remarkably increased peak separation (ΔE_p: 350 mV). However, the nano-Ni–SnO_2 modified electrode exhibited improved electron transfer property which facilitates the redox reaction of the probe. This resulted in the CV with reduced peak separation (ΔE_p: 190 mV) compared to that of pristine nano-SnO_2 (ΔE_p: 350 mV). The larger peak separation was assumed to result from the low electrical conductivity. Further, the BET surface area analysis showed increase in surface area for 1 wt% Ni doped nano-SnO_2 (40.128 m^2/g) compared to that of pure SnO_2 (23.20 m^2/g). These results clearly indicate Ni doping into SnO_2 remarkably increases the electron transfer property as well as the surface area.

Fig. 3(C) and (D) show various CVs recorded at different scan rates (10–100 mV/s) for pristine SnO_2 and nano-Ni–SnO_2 modified electrodes in 0.1 M KCl containing 1 mM of $[Fe(CN)_6]^{3-/4-}$. It can be seen that the anodic potential shifts towards positive side and the cathodic peak potential shifts in the reverse direction. Besides this, the redox peak currents are proportional to the square root of scan rate (inset of Fig. 3) which indicates diffusion electron-transfer process. It can be noticed that the redox potential of pristine SnO_2 modified electrodes shifts toward the higher side than that of 1 wt% Ni doped SnO_2 modified electrode. These observations suggest that the electron transfer rate of the nano-Ni–SnO_2 sample is higher than that of pristine sample.

The surface concentration of the nano-SnO_2 film can be estimated from the plot of current versus potential (*CV*) using Brown–Anson model that is based on the following equation

$$I_p = n^2F^2I^*AV/4RT$$

where n is the number of electrons transferred, F is the Faraday constant (96, 485 C mol^{-1}), I^* is the surface concentration (mol cm^{-2}). A is the surface area of the electrode (0.07 cm^2),

V is the scan rate ($10\,mV\,s^{-1}$), R is the gas constant ($8.314\,J\,mol^{-1}\,K^{-1}$) and T is the absolute temperature (298 K). The value of the surface concentration of the pristine SnO_2 and nano-Ni–SnO_2 modified electrodes have been estimated as 9.124×10^{-9} and $11.177\times10^{-9}\,mol\,cm^{-2}$ respectively. The difference in surface concentrations on GC electrode clearly indicates that the nano-Ni–SnO_2 has lower particle size compared to that of undoped nano-SnO_2. These results are in agreement with the average particle size estimated from powder XRD data.

3.4. Electrochemical behavior of HRP/SnO_2 modified electrodes

The cyclic voltammograms of a (a) HRP, (b) HRP/nano-SnO_2, and (c) HRP/nano-Ni–SnO_2 modified GC electrodes in nitrogen saturated 0.1 M PBS (pH 7.0) are shown in Fig. 4(A). Compared to those obtained at bare and HRP/nano-SnO_2 modified GC electrode, remarkably larger peak current was obtained at the HRP/nano-Ni–SnO_2 modified GC electrode. In addition, a pair of well defined redox peaks at the formal potential of -395 ± 3 mV has been obtained, which is nearly similar to that of -377 mV reported for HRP entrapped within a solid polymer matrix on a GCE (Ferri et al., 1998). This redox process featured nearly symmetric reduction and oxidation peaks. Obviously it was the electroactive center of HRP that performed the redox reaction at the HRP/nano-Ni–SnO_2 modified GC electrode. The results suggest that the HRP molecules entrapped in the nano-Ni–SnO_2 modified electrode retained the electrochemical activity. Further, the same GC electrode and undoped nano-SnO_2 modified GC electrode with HRP gave smaller redox peak currents compared to that of nano-Ni–SnO_2 modified GC electrode. It was also noted that neither the bare GC electrode nor the metal oxide modified GC electrode gave any peaks. According to Faraday's law $Q=nFA\Gamma^*$, where F is Faraday's constant, A is the geometrical surface area of the electrode, n is the number of electrons transferred and Q is the charge by integrating the cathodic peak of HRP at the CV. The surface concentration of electroactive HRP at the HRP/nano-Ni—SnO_2 modified GC electrode was estimated as $3.374\times10^{-10}\,mol\,cm^{-2}$ by assuming a one-electron transfer reaction. This value is higher than those of HRP at bare ($1.599\times10^{-10}\,mol\,cm^{-2}$) and nano-$SnO_2$ ($1.628\times10^{-10}\,mol\,cm^{-2}$). Besides, the nano-Ni–$SnO_2$ based electrode presented a much higher surface concentration of electroactive HRP than that of electrode without Ni doping. It may due to the high surface area ($40.128\,m^2/g$) for nano-Ni–SnO_2 compared to that of pristine SnO_2 ($22.0\,m^2/g$) as revealed by the BET surface analyses. As a result, the higher current response and larger concentration of electroactive HRP should be associated with large surface-to-volume ratio and Ni doping on SnO_2 nanoparticles.

Fig. 4(B) shows the CVs of HRP/nano-Ni–SnO_2 modified glassy carbon electrode with different scan rate (100–1000 mV/s) in nitrogen saturated PBS (pH 7.0). The redox process of this modified electrode was a typical quasi-reversible electrochemical process involving an active substance attached to the electrode. The results indicate that all the electroactive HRP Fe(III) in nano-Ni–SnO_2 modified electrode were reduced to HRP Fe(II) on the forward scan and then re-oxidized to Fe(III) on the reverse scan (Chen et al., 2000). Further, both the oxidation and reduction peak heights of the redox processes were found to increase linearly with square root of scan rate from 100 to 1000 mV/s. The regression equation

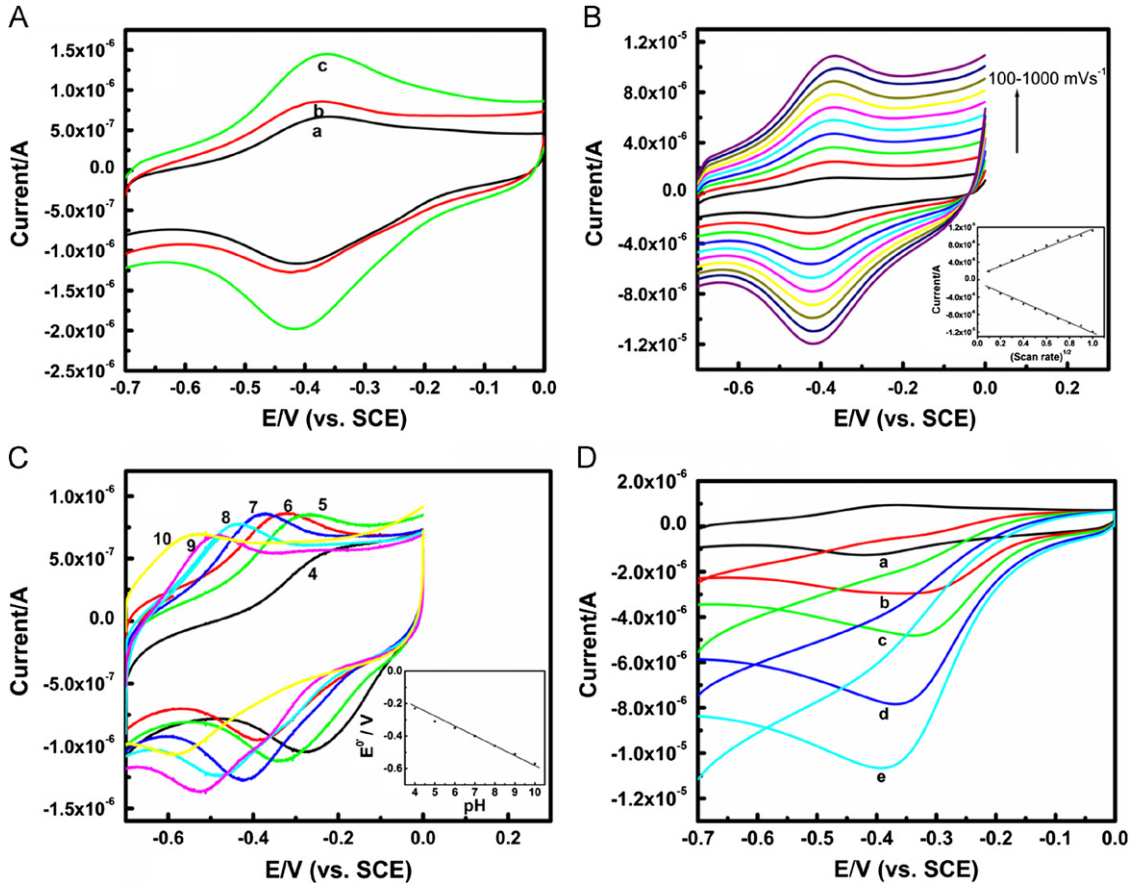

Fig. 4. (A) CVs of HRP on (a) bare, (b) nano-SnO_2, and (c) nano-Ni–SnO_2 recorded in 0.1 M. PBS (pH 7.0) at a scan rate of 100 mV/s in the potential range between -0.7 and 0.0 V. (B) CVs of HRP/nano-Ni–SnO_2 modified GC electrode at different scan rate (100–1000 mV/s) in PBS. (C) CVs of HRP/nano-Ni–SnO_2 modified electrode in 0.1 M PBS; scan rate (100 mV/s). Inset shows plot of peak potential vs. pH. (D) CVs of HRP/nano-Ni–SnO_2 modified electrode in the absence (a) and presence of (b) 50 μM, (c) 100 μM, (d) 300 μM and (e) 500 μM of H_2O_2 in 0.1 M PBS (pH 7.0); scan rate: 100 mV/s.

was deduced as I_{pa} (μA)=1.02 (V s^{-1})+1.310, r=0.994; I_{pc} (μA)= −1.08 (V s^{-1})–1.310, r=0.998. According to $I_p=nFQv/4RT$ and $E_p=-RT/F$ lnKs (Srinivasan and Gileadi, 1966; Sharp et al., 1979) the derived number of electrons n and average apparent heterogeneous electron transfer rate constant k_s corresponded to 0.92 and 1.10 s^{-1}, respectively (F, R, T have their usual significance; I_p is peak current; E_p is peak potential; Q is charge involved in the reaction and v is scan rate (V/s)). The characteristics of this redox reaction involving the electroactive center of HRP corresponded to those of other heme-containing proteins including myoglobin, hemoglobin, cytochrome P450 and HRP. These results revealed that the electron transfer between HRP and GC is a surface-controlled electrochemical process and the immobilized HRP on nano-Ni–SnO_2 is not denatured.

The effect of pH on the electrochemical behavior of HRP in nano-Ni–SnO_2 modified electrode has been examined by cyclic voltammetry. The CV peaks for HRP/nano-Ni–SnO_2 modified surface shifted negatively with increasing pH (Fig. 4(C)). Further, the results show that the electrode potential of the redox peaks strongly depends on the pH of the electrolytes. All changes in CV peak potentials and currents with pH were reversible. The plot of formal potential (E^0) versus pH was linear with slope of about −54 mV per pH unit (inset in Fig. 5). The regression equation is derived as E^0(U)= −0.054 pH= +0.0218 with regression coefficient of 0.9978. The slope was close to the expected value of −57.8 mV per pH indicating that one proton participated in the electron-transfer process for neutralizing the charge change during redox reaction (Sun et al., 2000). Moreover, the change of solution pH did not affect the peak-to-peak separation; thus, the diffusion of proton in the enhanced tri-helix scaffold of nano-Ni–SnO_2 was very fast. It further confirms that the responses of the HRP/nano-Ni–SnO_2 biosensors are due to the redox reaction of the immobilized HRP on the electrode surface. In order to provide a favorable microenvironment of HRP, pH 7.0 was chosen.

3.5. Performance of the HRP/nano-Ni–SnO_2 film based hydrogen peroxide biosensor

The modified HRP/nano-Ni–SnO_2 showed good electrocatalytic activity towards H_2O_2 reduction. Fig. 4(D) shows the CVs of the HRP/nano-Ni–SnO_2 modified electrode in a solution containing different concentration of hydrogen peroxide under the condition of nitrogen saturation. When H_2O_2 was added into pH 7.0 PBS, there is a significant increase in the cathodic peak at about −0.4 V and decrease in the anodic peak current. It was also noted that neither the bare GC electrode nor the metal oxide modified electrode revealed similar phenomena. So the catalytic reduction of H_2O_2 was due to the immobilized HRP in the nano-Ni–SnO_2, which provide a fast direct electron transfer reaction between the heme of HRP and the electrode surface. The heme can react with H_2O_2 to form a first intermediate of compound I, which has catalytic activity to H_2O_2. The catalytic procedures can be explained as follows (Zhang et al., 2004).

$$\text{HRP } (Fe^{3+}) + H_2O_2 \rightarrow \text{compound I } (Fe^{4+}=O) + H_2O \quad (1)$$

$$\text{Compound I } (Fe^{4+}=O) + e + H^+ \rightarrow \text{compound II} \quad (2)$$

$$\text{Compound II} + e + H^+ \rightarrow \text{HRP } (Fe^{3+}) + H_2O \quad (3)$$

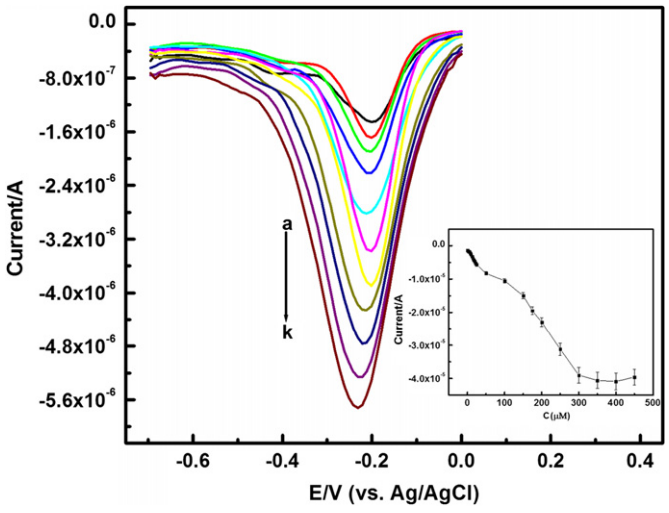

Fig. 5. (A) Differential pulse voltammograms of the HRP/nano-Ni–SnO_2 modified GC electrode in nitrogen saturated PBS (pH 7.0) with various concentration of H_2O_2 (a–k) 0, 1.0×10^{-7}, 2.5×10^{-6}, 5.0×10^{-6}, 7.5×10^{-5}, 1.0×10^{-5}, 1.25×10^{-5}, 1.50×10^{-5}, 1.75×10^{-5}, 2.0×10^{-5}, 2.5×10^{-5} M; scan rate (10 mV/s); modulation amplitude 25 mV. Inset shows the corresponding calibration plots of DPV response toward H_2O_2.

Electrocatalytic reductions of hydrogen peroxide were examined using differential pulse voltammetric (DPV) method which is one of the most widely employed techniques for biosensors. The DPV is a pulse technique which allows much higher sensitivity than conventional sweep techniques when detecting very low concentrations of an analyte. This is achieved by applying a small voltage pulse superimposed on the linear voltage sweep and sampling the differential current at a short time after pulse. Hence, the measured current is only a product of the Faradic process, with the capacitive charging current eliminated. Fig. 5 shows the DPVs of HRP/nano-Ni–SnO_2 modified GC electrode (pH 7.0 PBS) for different concentration of H_2O_2. Here the DPVs were recorded by sweeping the potential between −0.7 and 0.0 V at modulation amplitude of 25 mV, and a scan rate at 10 mV/s. In Fig. 5, curves a–k shows the well-defined and stable cathodic reduction peak current curves for H_2O_2 reduction. These demonstrated that the nano-Ni–SnO_2 modified electrode might provide a good microenvironment for investigating the fast electrode process kinetics. The corresponding calibration curve is presented in the inset of Fig. 5. The catalytic reduction peak current increased linearly with the H_2O_2 concentration in a linear range from 1.0×10^{-7} to 3.0×10^{-4} M with a correlation coefficient of 0.9897. When the H_2O_2 concentration was higher than 3.3×10^{-4} M, the calibration curves tended to a plateau, which is a typical Michaelis–Menten kinetics behavior. The apparent Michaelis–Menten constant (K_M^{app}) was estimated to be 0.221 mM using the Lineweaver–Burk equation. The small K_M^{app} constant shows a high affinity to H_2O_2 and good bioactivity of the HRP/nano-Ni–SnO_2 toward H_2O_2 reduction. The detection limit of the fabricated biosensor was examined to be 4.3×10^{-8} M. The main advantage is that the metal oxide preparation, electrode modification and finally enzyme immobilization employed in the present study is very simple when compared to the reported tedious procedures. The performance of the fabricated biosensor was very much comparable to the literature values (Supplementary, Table 1). The comparative data suggests superiority of the present sensor over some reported H_2O_2 biosensors, the possible reason being that the nano-Ni–SnO_2 modified surface possesses a good electron transfer property. Further, the high surface area (40.128 m^2/g) of nano-Ni–SnO_2 can hold large amount of enzyme which might provide better communication between enzyme and electrode. In addition, this nano-Ni–SnO_2 modified surface provides a friendly micro-environment to retain HRP bioactivity.

3.5.1. The stability and reproducibility of the obtained electrode

The storage stability of the HRP/nano-Ni–SnO_2 modified GCE was also investigated. The cathodic peak current was measured using the same electrode and it retained above 97% of its initial response stored at 4 °C after 1 week. Further, the direct electron transfer of HRP is stable. The cyclic voltammetric responses of the HRP-nano-

Ni–SnO_2 modified electrode in N_2-saturated PBS (pH=7.0) show no obvious changes after 20 cycles, and then it decreases (2.835%) slowly with the increase in cycles up to 100 (data not shown here). The reproducibility of the biosensor was investigated using 100 μM H_2O_2, with a series of five DPV experiments and the relative standard deviation (R.S.D) of 4.26% was achieved. These results indicated that the immobilized HRP possesses high enzymatic activity and nano-Ni–SnO_2 provided favorable microenvironment for HRP to perform direct electron transfer at the modified electrode.

4. Conclusions

Single phase Ni doped SnO_2 nanoparticles were successfully synthesized by a simple microwave irradiation method. Powder XRD and TEM analyses confirmed the phase purity and nanometric dimension of the samples. The grain sizes have been found to get reduced with increase in Ni concentration. Magnetic measurements revealed that the 1 wt% Ni doping into SnO_2 did not affect its diamagnetic behavior, but the higher Ni concentration (5 wt%) caused ferromagnetism in SnO_2. This result is important in view of the fact that the higher Ni doping did not promote the sensing characteristics of nano-Ni–SnO_2. Using this metal oxide nanoparticles incorporated with HRP, we have fabricated a simple and novel differential pulse voltammetric hydrogen peroxide biosensor. The electrochemical behavior of HRP at the nano-Ni–SnO_2 modified electrode demonstrated the direct electron transfer reaction of HRP. The fabricated biosensor exhibits good affinity, fast response, wide linear range, lower detection limit, high sensitivity, operational convenience, storage stability and acceptable reproducibility. The results indicated that the Ni doped SnO_2 nanoparticles can provide a favorable microenvironment for the enzyme and promote the direct electron transfer at the electrode surface.

Acknowledgment

The authors thank the University Grants Commission (F.no. 40-2/2011) for financial support.

Appendix A. Supporting information

Supplementary data associated with this article can be found in the online version at http://dx.doi.org/10.1016/j.bios.2012.03.035.

References

Ahmed, S.A., 2010. Solid State Communications 150, 2190–2193.
Ahn, H.J., Choi, H.C., Park, K.W., Kim, S.B., Sung, Y.E., 2004. The Journal of Physical Chemistry B 108, 9815–9820.
Ansari, A.A., Alhoshan, M., Alsalhi, M.S., Aldwayyan, A.S., 2010. Biosensors., pp. 302.
Ansari, A.A., Solanki, P.R., Malhotra, B.D., 2009. Journal of Biotechnology 142, 179–184.
Aragon, F.H., Coaquira, J.A.H., Hidalgo, P., Brito, S.L.M., Gouvea, D., Castro, R.H.R., 2010. Journal of Non-Crystalline Solids. 356, 2960–2964.
Cao, D., Hu, N., 2006. Biophysical Journal 121, 209–217.
Chen, X., Ruan, C., Kong, J., Deng, J., 2000. Analytica Chimica Acta 412, 89–98.
Chu, D., Masuda, Y., Ohji, T., Kato, K., 2011. Chemical Engineering Journal 168, 955–958.
Ferapontova, E., Schmengler, K., Borchers, T., Ruzgas, T., Gorton, L., 2002. Biosensors and Bioelectronics 17, 953–963.
Ferri, T., Poscia, A., Santucci, R., 1998. Bioelectrochemistry and Bioenergetics (Lausanne, Switzerland) 44, 177–181.
Hidalgo Falla, M.P., Peres, H.E.M., Ramirez-F, F.J., 2004. Physica Status Solidi (c) 1, S112–S115.
Jain, K., Pant, R.P., Lakshmikumar, S.T., 2006. Sensors and Actuators B 113, 823–829.
Janasek, D., Spohn, U., Beckmann, D., 1998. Sensors and Actuators B 51, 107–113.
Kafi, A.K.M., Wu, G., Chen, A., 2008. Biosensors and Bioelectronics 24, 566–571.
Kang, S.Z., Yang, Y., Mu, J., 2007. Colloids Surface A 298, 280–283.
Korotcenkov, G., Do Han, S., 2009. Materials Chemistry and Physics 113, 756–763.
Li, L., Huang, J., Wang, T., Zhang, H., Liu, Y., Li, J., 2010a. Biosensors and Bioelectronics 25, 2436–2441.
Li, Y., Zhang, J., Xuan, J., Jiang, L., Zhu, J., 2010b. Electrochemistry Communications 12, 777–780.
Lin, K.C., Tsai, T.H., Chen, S.M., 2010. Biosensors and Bioelectronics 26, 608–614.
Lobnik, A., Cajlakovic, M., 2001. Sens. Actuators B 74, 194–199.
Lu, X., Zhang, H., Ni, Y., Zhang, Q., Chen, J., 2008. Biosensors and bioelectronics 24, 93–98.
Sambasivam, S., Chun Choi, B., Lin, J.G., 2011. Journal of Solid State Chemistry 184, 199–203.
Sharp, M., Petersson, M., Edstrom, K., 1979. Journal of Electroanalytical Chemistry 95, 123.
Song, M., Jiang, H., Wang, X., Ge, L., 2010a. Journal of Applied Polymer Science 117, 1613–1617.
Song, M.-J., Hwang, S.W., Whang, D., 2010b. Journal of Applied Electrochemistry 40, 2099–2105.
Srinivasan, S., Gileadi, E., 1966. Electrochimica Acta 11, 321–335.
Sun, H., Hu, N., Ma, H., 2000. Electroanalysis 12, 1064–1070.
Tian, Z.M., Yuan, S.L., He, J.H., Li, P., Zhang, S.Q., Wang, C.H., Wang, Y.Q., Yin, S.Y., Liu, L., 2008. Journal of Alloys and Compounds 466, 26–30.
Wan, J., Bi, J., Du, P., Zhang, S., 2009. Analytical Biochemistry 386, 256–261.
Xiao, P., Garcia, B.B., Guo, Q., Liu, D., Cao, G., 2007. Electrochemistry Communications 9, 2441–2447.
Yin, H., Ai, S., Shi, W., Zhu, L., 2009. Sensors and Actuators B 137, 747–753.
Zhang, L., Ge, S., Zuo, Y., Wang, J., Qi, J., 2010. Scripta Materialia 63, 953–956.
Zhang, Y., He, P., Hu, N., 2004. Electrochimica Acta 49, 1981–1988.